Journal of Photochemistry and Photobiology A: Chemistry 200 (2008) 294–300

Contents lists available at ScienceDirect

Journal of Photochemistry and Photobiology A: Chemistry

journal homepage: www.elsevier.com/locate/jphotochem

Influence of light scattering particles in the TiO_2 photoelectrode for solid-state dye-sensitized solar cell

Soon Hyung Kang[a], Jae-Yup Kim[a], Hyun Sik Kim[a], Haeng-Deog Koh[b], Jae-Suk Lee[b], Yung-Eun Sung[a,*]

[a] School of Chemical & Biological Engineering & Interdisciplinary Program in Nano Science and Technology, Seoul National University, Seoul 151-744, Republic of Korea
[b] Department of Materials Science and Engineering, Gwangju Institute of Science and Technology, Gwangju 500-712, Republic of Korea

ARTICLE INFO

Article history:
Received 4 January 2008
Received in revised form 19 May 2008
Accepted 15 August 2008
Available online 29 August 2008

Keywords:
Light scattering particle
Solid-state dye-sensitized solar cell
Polymer beads

ABSTRACT

A TiO_2 film was modified by adding light scattering particles and applied to an anode electrode in solid-state dye-sensitized solar cells (DSSCs). The TiO_2 films with 10 wt% (vs. TiO_2 weight) light scattering particles showed enhanced performance (28%), compared with nanocrystalline TiO_2 films, which were used as the controls. In particular, the photocurrent density (J_{sc}) reached approximately 12.6 mA/cm^2 under a one-sun condition. This was attributed to the light scattering effect and decrease in internal resistance through the macroporous structure with a minor loss of electron transport. However, in the case of a larger concentration of light scattering particles (>10 wt%), there was a decrease in the efficiency of DSSCs, which resulted from the decreased surface area and degraded electron transport and charge recombination properties, as confirmed by the measurement of stepped light-induced photocurrent and photovoltage transients. Furthermore, the diffusion properties and kinetics of the composite polymer electrolyte with the nanoporous and macroporous TiO_2 films were compared and evaluated from the electrochemical impedance spectra.

1. Introduction

Recently, there has been considerable attention concentrated on dye-sensitized solar cells (DSSCs) composed of nanoporous TiO_2 particles [1]. As a promising alternative energy device to conventional Si solar cells, the combination of clean and unlimited solar energy as well as low production costs can allow commercialization of DSSCs, even though the conversion efficiency should be >11%. For the production of commercial DSSCs, liquid electrolyte-based DSSC should be substituted for solid- or quasi-solid type electrolyte-based DSSC due to their many practical limitations, such as dye desorption, solvent evaporation resulting from imperfect sealing of the cell, cell degradation by reactions between permeated water/oxygen and the electrolyte, and high temperature instability [2–4]. In this regard, enormous effort has moved to solid- or quasi-solid type electrolyte materials.

Recently, the Grätzel group [5] reported quasi-solid-state DSSCs with high efficiency (7.5%) employing a composite ionic liquid-based electrolyte. The high conversion efficiency was explained by the increased conductivity of I_3^- ions in the viscous solvent resulting from an increase in the range of the amorphous phases after SiO_2 or TiO_2 nanoparticles (in size of 15–20 nm) had been inserted [6]. Accordingly, the simple procedure for preparing a composite polymer electrolyte is expected to inject new momentum into new fields, such as electrochromic devices [7], polymer batteries [8,9], and fuel cells [10]. Unlike the operation of a liquid electrolyte, the mass transport of the charge carrier in the viscous polymer electrolyte is controlled by ion diffusion, which relies mainly on the diffusion coefficient of I_3^- ions and the viscosity of the solvent, and is affected slightly by the structure of the porous TiO_2 film electrode. This is because a porous and three-dimensional TiO_2 network obstructs the diffusion of electroactive species to the surroundings of a close substrate [4].

In addition, the effective internal surface area of a nanocrystalline TiO_2 film is approximately one thousand times higher than that of a flat TiO_2 film, which has a significant effect on the light harvesting yield. However, the conversion efficiency begins to degrade above limited certain point because the relationship between the specific surface area and photocurrent in a nanoporous TiO_2 film is not proportional. The commercial dye (N719) molecules used show particularly poor absorption ability of solar light, especially in the longer wavelength range λ = 600–800 nm. Therefore, many different dyes have been investigated in an attempt to extend the spectral response toward a longer wavelength range. However, many synthesized dyes have limited utility [12,13]. Hence, modification of the TiO_2 working electrode with larger TiO_2 nanoparticles (~200 nm), which behave as light scattering particles (LS), was attempted with

* Corresponding author. Tel.: +82 2 880 1889; fax: +82 2 888 1604.
E-mail address: ysung@snu.ac.kr (Y.-E. Sung).

1010-6030/$ – see front matter © 2008 Elsevier B.V. All rights reserved.
doi:10.1016/j.jphotochem.2008.08.010

the aim of extending the spectral wavelength range for light absorption by increasing the optical path length. Recently, Wan In Lee and co-workers reported that a nano-embossed hollow spherical TiO_2 particle-based photoanode with bifunctional properties improved the conversion efficiency (21% increase), compared with that of a 400 nm-diameter scattering particle-based photoanode. This was attributed to the light scattering effect of large nano-embossed hollow spheres in the longer wavelength region and the generation of photo-excited electrons because the walls of the obtained hollow spheres were composed of nanocrystalline anatase TiO_2 particles [14]. In addition, TiO_2 electrodes with microtube-network structures showed enhanced photovoltaic performance (30%) compared to that of nanocrystalline TiO_2 films using an ionic liquid type electrolyte [15]. Herein, the main contributing factors were the extension of the light path length (light scattering effect) and decrease in the transport resistance (macroporous structure). Similarly, in the situation where ion diffusion in the viscous polymer electrolyte becomes problematic, the random distribution of light scattering particles might promote the favorable penetration of a viscous polymer electrolyte into a nanoporous TiO_2 film. It should be noted that too many large particles might significantly reduce the internal surface area, resulting in lower conversion efficiency. In addition, photoinjected electrons should experience frequent trapping/detrapping events that would limit transport through the nanoporous TiO_2 layer due to the reducing electron diffusion length.

Therefore, this study investigated the effects of a suitable mixture of small particles, which would have a large effective internal surface, and larger particles, which would be effective light scattering agents, on a modified TiO_2 electrode for applications to solid-state DSSCs.

2. Experimental

An optically transparent conducting glass (FTO (fluorine doped SnO_2), Pilkington TEC Glass™, sheet resistance 8 Ω/sq, transmittance 77% in the visible range) was used as the substrate. The substrate was cleaned sequentially in acetone, ethanol and deionized (DI) water for 20 min in each step to remove the organic pollutants. The TiO_2 electrode as a control sample was fabricated as reported in a previous paper [16]. The modified sample showed more efficient performance due to the increased porosity and specific surface area, which are associated with an increase of the photocurrent of the cell. Furthermore, a somewhat uniform pore distribution was obtained. More detailed results and discussion are reported elsewhere [11].

TiO_2 powder (0.6 g), 1 wt% Vulcan spherical carbon nanopowder with a 30 nm particle size as a porosity inducing material, and light scattering particles (ST1, Ishihara Sanyo, Japan) ranging in size from a length of 200 nm and a width of 50 nm were mechanically ground together. Subsequently, acetylacetone, polyethylene oxide, and solvent (water/ethanol) were added. The quantity of light scattering particles incorporated in TiO_2 was controlled. A black colored TiO_2 film was made from the paste using a doctor blade technique, and dried for 5 min using a hot air dryer. The thermal treatment in the second-step (450 °C for 30 min → 550 °C for 30 min) was performed to completely remove the incorporated elemental carbon through a chemical reaction with oxygen.

For the formation of large pores and an increase in light scattering [17] in the nanoporous TiO_2 film, the polymer beads were synthesized using a methyl metacrylate (MMA) monomer by emulsion polymerization. The beads were spherical approximately70 to 100 nm in radius [18]. A surface functional group on the polymer beads was a substituted hydrophilic chain that was soluble in water-based solvents. The concentrated polymer bead was diluted in water to a ratio of 1:20 by volume.

After a high temperature thermal treatment for a short time, the polymer beads were burnt out leaving a reverse structure or polymer bead-sized pores in the TiO_2 films. The thickness of the TiO_2 film was controlled using transparent adhesive tape (Scotch, nominal thickness: 50 μm) as a spacer and was measured to be approximately 4.7 μm (±0.5 μm) using an Alpha-Step 200 apparatus (Tencor Instruments).

For the adsorption of the dye, the baked electrodes were immersed in an ethanol solution containing 5×10^{-4} M *cis*-bis (isothiocyanato)bis(2,2′-bipyridy-4,4′-dicarboxylato)-ruthenium (II) bis-tetrabutylammonium (Ru 535-bisTBA, Solaronix) for approximately 12 h at room temperature. The electrode was then rinsed with ethanol and dried under an air stream. The polymer electrolyte was composed of a low molecular weight poly(ethylene oxide dimethyl ether) (PEODME, M_w = 500 g/mol, R_g = 1.4 nm), fumed silica nanoparticles (20 nm, Degussa), 1-methyl-3-propyimidazolium iodide, iodine, and acetonitrile as the volatile solvent [19]. The composite solution was stirred for 12 h and the solvent was evaporated in an oven at 60 °C. In the case of the silica nanoparticle inserted polymer electrolyte, the improved ionic conductivity and a high interfacial contact resulted in improved conversion efficiency. Pt-coated counter electrodes were prepared by spreading a drop of 10 mM H_2PtCl_6 in 2-propanol onto the FTO glass and heating it to 400 °C for 20 min under air ambient. Only one-side of the dye-adsorbed TiO_2 electrodes (active area 0.16 cm^2) was pressed using the thermal adhesive films (Serlyn, thickness: 60 μm), which controlled the thickness of the polymer electrolyte. Finally, the polymer electrolyte solution was cast on the TiO_2 electrode, which was covered by the Pt-coated counter electrode.

The absorbance spectra were investigated using a Shimadzu model 3100 UV–vis (ultraviolet–visible) spectrophotometer over the wavelength range, 500–1000 nm, at room temperature. The photocurrent–voltage (*J*–*V*) measurements were performed using an XIL model 05A50KS source measurement unit at a power of 100 mW/cm^2. A 500-W Xenon lamp was used as the light source and its light intensity was calibrated to AM 1.5 radiation (one-sun condition) using a NREL fabricated Si reference solar cell. The light was homogenous up to 5 cm × 5 cm.

The stepped light-induced measurements of the photocurrent and voltages transients (SLIM-PCV) were used to measure the electron diffusion coefficient (D), which was correlated to the electron transport in the TiO_2 film, and the electron lifetime (τ), which was related to the extent of charge recombination. The transient photocurrent and photovoltage were deduced by a stepwise change in the intensity of a 632 nm laser pulse stepped down by ND filters to 10 mW/cm^2. The D values were obtained by the time constant (τ_c), which was determined by fitting an exponential function of the photocurrent transient with exp ($-t/\tau_c$), according to the following equation, $D = \omega^2/(2.35\tau_c)$ with a TiO_2 film thickness (w). In addition, the τ values were derived by fitting an exponential function of the photovoltage transient to exp($-t/\tau$) [20,21].

The photocurrent action spectra (IPCE) were collected under short circuit conditions with a tungsten lamp source and a 20 nm bandwidth monochromator, resulting in an illumination intensity of approximately 1 mW/cm^2.

The electrochemical impedance spectra were obtained by applying a sinusoidal perturbation of ±5 mV over an open-circuit voltage at frequencies ranging from 0.01 Hz to 100 kHz in the dark or under illumination (AM 1.5, one-sun condition) using a Zahner impedance analyzer to examine the diffusion properties and ionic conductivity in the polymer electrolyte. The measurements were also used to

determine the origin of the resistive losses in the nanoporous TiO_2 film.

3. Results and discussion

Fig. 1 shows the absorbance spectra of the TiO_2 films containing the light scattering particles and polymer beads. The incorporated polymer beads were well dispersed in the TiO_2 colloidal paste at a 1:20 ratio by weight. However, there was no change in the absorbance as the spherical polymer beads were incorporated in the TiO_2 film, which means that there was no light scattering effect from the inserted polymer beads due to the small size distribution from 70 to 100 nm.

One might expect the incorporated polymer beads to decrease the internal surface area due to the increase in porosity and the formation of a sparsely interconnected TiO_2 particle network, which would decrease the photocurrent density. On the other hand, the Kern group [22] reported that the dimensions of backscatterers generating effective Mie scattering were approximately 50–100 nm in radius and the solid particles were 50–700 nm in radius, assum-

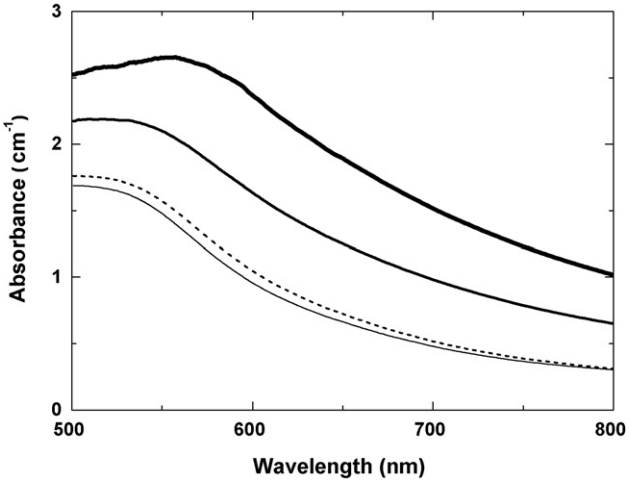

Fig. 1. UV–vis spectra of the dye-adsorbed TiO_2 film containing light scattering particles (10 wt% (—), 20 wt% (▬) vs. TiO_2 weight and 5 wt% polymer beads (···) (20 vol% diluted in water)). The control sample was described with the dashed line.

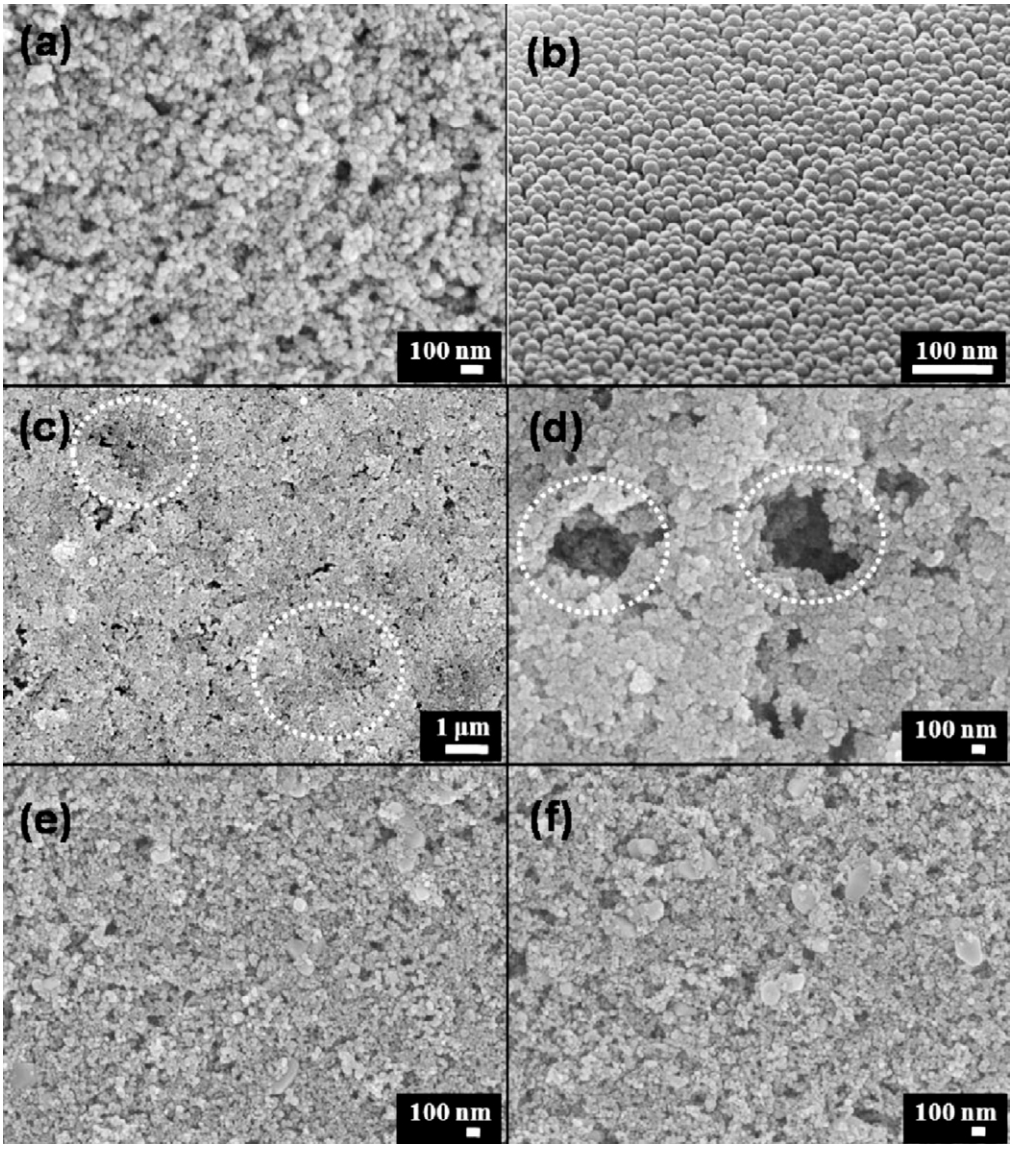

Fig. 2. FE-SEM images; (a) TiO_2 film (control sample), (b) synthesized polymer beads, (c) modified samples containing 5 wt% polymer beads, (d) the magnified view of (c) image, (e) modified sample containing 10 wt% light scattering particles, and (f) modified sample containing 20 wt% light scattering particles.

ing that Mie theory applies to an isotropic and homogenous sphere [23]. Although the reported void dimensions are similar to those in this experiment, there was no light scattering effect in the longer wavelength range. The latter effect might be due to the high specific surface area and porosity that already exist in the TiO_2 samples used.

The incorporation of solid light scatterers was found to influence the absorbance of dye-adsorbed TiO_2 film in the longer wavelength region. The maximum wavelength of the absorbance was shifted to a longer wavelength (560–590 nm) with increasing amount of incorporated solid light scattering particles. Moreover, the intensity of the absorbance was increased. This can be explained from the light scattering effect of the 200 nm-sized TiO_2 particles. In addition, it should be noted that light scattering relies on a change in the refractive index at the interface between the materials. The effective medium between the active layer of TiO_2 (effective refractive index (η) = 2.5) and the electrolyte (η = 1.6), is sufficient to show a light scattering effect at the interface [24]. However, a large fraction of light scattering particles is needed for effective light scattering, which will lead to a simultaneous decrease in effective surface area. This effect will be discussed in the next section.

Fig. 2 shows FE-SEM images of the surface of the TiO_2 film containing the solid light scattering particles and polymer beads. The TiO_2 film (control sample) in Fig. 2(a) shows a nanoporous structure with a uniform pore distribution (~30 nm) [11]. The sample containing 5 wt% polymer beads diluted 10% by volume (abbreviated as 5 wt% PB sample) showed random bulky-sized pores and a crater-shaped dented morphology at the surface, which is highlighted by the white circles in Fig. 2(c) and (d).

From Fig. 2(b), the synthesized polymer beads were found to have a uniform size ranging from 70 to 100 nm with a spherical shape. The TiO_2 sample containing 10 wt% solid light scattering particles (abbreviated as 10 wt% LS sample) shows a rough and uneven surface morphology, compared with the control sample, as shown in Fig. 2(e). Increasing the content of light scattering particles (20 wt%) caused a rough surface morphology, which was similar to the 10 wt% LS sample (Fig. 2(f)). The extreme rugged surface morphology might cause the loss of electron transport in the nanoporous TiO_2 film [25], which should degrade the conversion efficiency of DSSC as a result of charge recombination. Furthermore, the back scattering from the light scattering thin film also decreases the efficiency as a result of the loss of incident solar light. The incorporated solid light scattering particles exhibit a laminar structure with a long round shape along the *c*-axis. It was evident that these large nanoparticles might affect not only the permeation of the polymer electrolyte but also light scattering in the near-IR region.

The photovoltaic performance of the control sample and modified sample was tested, as shown in Fig. 3(a). The 10 wt% LS sample showed the best efficiency of 4.75%, while the 5 wt% PB sample showed lower conversion efficiency than the control. It appears that the decrease in internal surface area makes a more important contribution to the efficiency than the light scattering effect. Therefore, the conversion efficiency decreased with increasing content of light scattering particles incorporated. These results suggest that 10 wt% LS particle inserted film is most suitable for enhancing the solar absorption. Fig. 3(b) shows the incident photon on the electron efficiency (IPCE) of the 10 wt% LS sample and control sample. The IPCE value corresponds to the number of electrons generated by monochromatic light in the external circuit divided by the number of incident photons. In the case of the 10 wt% LS sample, the IPCE corresponds to the absorption wavelength of the dye used, and was as high as 60% at 530 nm with slightly higher conversion efficiency at the longer wavelengths of 600–800 nm. This confirms the results of the UV–vis spectra, which was attributed to the scattering effect of the larger particles.

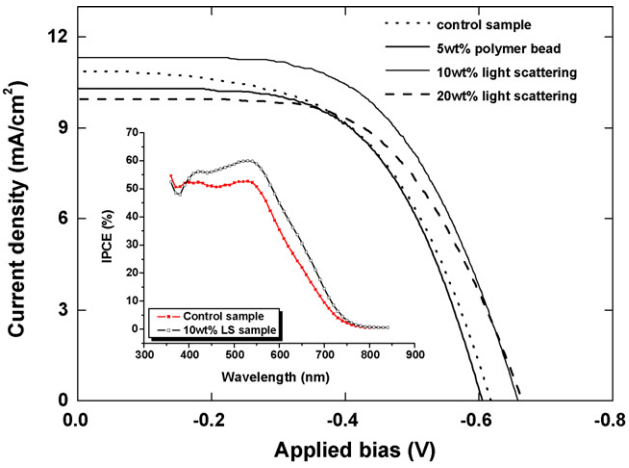

Fig. 3. (a) *J–V* characteristics under AM 1.5 illumination of 100 mW/cm^2. The samples with 5 wt% polymer beads (···), 10 wt% light scattering particles (—), 20 wt% light scattering particles (▬), and control (—·—) are shown. The active area was approximately 0.16 cm^2. (b) IPCE spectra of the DSSCs as a function of the wavelength. The control sample (●) and 10 wt% LS sample (○) are shown. The fabricated active area was approximately 0.36 cm^2.

It should be noted that the significant increase in light absorbance at the longer wavelengths shown in Fig. 1 does not entirely control the increase in photocurrent density. Related analysis should be performed to determine the cause in the next paragraph. Table 1 summarizes the *J–V* characteristics. The 10 wt% LS sample shows a V_{oc}, J_{sc}, fill factor and efficiency of 0.651 V, 12.6 mA/cm^2, 57.8%, and 4.75%, respectively. Compared with the control sample, the higher V_{oc} was attributed to the favorable permeation of the solid polymer electrolyte, causing less charge recombination. The increased photocurrent might be induced by the increase in light absorption from the UV–vis spectra.

The IPCE value shows a minor light scattering effect, which supports the favorable permeation of the polymer electrolyte into the nanostructured TiO_2 film [16]. Moreover, the low fill factor was explained by a variety of factors, the main factor being the series resistance of the TCO (transparent conducting oxide) substrate due to long-term annealing and the diffusion of the solid-state polymer electrolyte into the nanoporous TiO_2 film.

In the case of the 5 wt% PB sample, the increased fill factor resulted from favorable permeation of the polymer electrolyte into the internal interface between the substrate and nanoporous TiO_2 layer. Nevertheless, the conversion efficiency was low due to the decrease in internal surface area as a result of the formation of bulky-pores, rather than by the light scattering effect, which would induce photocurrent degradation. The decrease in photovoltage originates from the significant loss of electron transport in the low coordination number of the thin film consisting of nano-sized TiO_2 particles linked to the increased charge recombination. Furthermore, there might be a minor effect from the intimate connection between the TCO substrate and polymer electrolyte. The enhanced

Table 1
The summary of the *J–V* characteristics for solid-state dye-sensitized solar cells (solar illumination intensity: 100 mW/cm^2)

	V_{oc} (V)	J_{sc} (mA/cm^2)	F.F (%)	η (%)
Control sample	−0.616	10.87	55.5	3.72
5 wt% PB	−0.604	10.31	59.2	3.68
10 wt% LS	*−0.651*	*12.6*	*57.8*	*4.75*
20 wt% LS	−0.676	10.9	57.7	4.27

The significance of italic characters mean the maximum conversion efficiency of solid-state dye sensitized solar cell

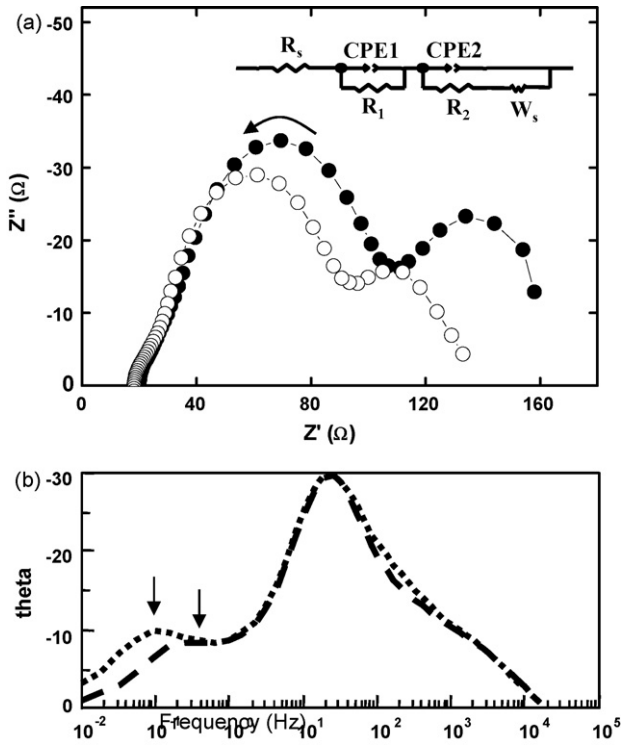

Fig. 4. Impedance spectra of the control sample and 10 wt% LS sample measured at the open-circuit voltage (−0.65 V) under solar illumination with the intensity of one-sun; (a) the Nyquist plots of control sample (●) and 10 wt% LS sample (○). The inset of (a) shows the equivalent circuit describing the interface in the solid-state DSSCs composed of FTO(substrate)/TiO_2-dye/polymer electrolyte/Pt-coated substrate. R_s: solution resistance, R_1 and R_2: charge transfer resistance at the counter electrode/electrolyte and the TiO_2/electrolyte, CPE1 and CPE2: constant phase element of capacitance corresponding to R_1 and R_2, respectively, W_s: finite Warburg impedance. (b) The Bode plots of the control sample (···) and 10 wt% LS sample (—-).

fill factor is linked to the rapid diffusion of the polymer electrolyte in the film assisted by the bulky-pores. Overall, the incorporation of polymer beads in the carbon-incorporated TiO_2 film is unsuitable for applications to solid-state DSSCs.

In order to determine the factors that influence the efficiency of the solid-state DSSC, the electrochemical impedance spectra with illumination (mentioned at Table 1) and in the dark (V_{oc} corresponded to 0.23 ± 0.1 V) were measured under the open-circuit condition, using a perturbation of ±5 mV/s, shown in Fig. 4. The Nyquist diagrams of the control and 10 wt% LS sample show similar curves depending on the frequency, with the exception of the indistinct appearance of a semicircle at high frequency. Referring to previous reported results [26,27], the charge transfer resistance at the electrolyte/Pt-coated counter electrode was associated with the high frequency range. The electron transport and electron capturing behavior of I_3^- at the TiO_2/electrolyte interface can be analyzed in the medium frequency range. In the low frequency range, the impedance properties should be related to the diffusion of I_3^- in the polymer electrolyte.

The control sample shows prominent diffusion related resistance of the polymer electrolyte and electron transport along with transfer related resistance in the nanoporous TiO_2 film/electrolyte, compared with the 10 wt% LS sample. In addition, the magnitude of the curve (Z'') increased. In the kinetic region, the 10 wt% LS sample showed a blue shift in the peak related to the electrolyte diffusion suggesting more rapid charge transfer than the control sample. This indicates that the films with solid light scattering particles facilitate diffusion into the nanostructured TiO_2 film.

The inset in Fig. 4(a) shows the equivalent circuit model of the impedance of a solid-state DSSC. R_s denotes the resistance of the polymer electrolyte and the TCO substrate. R_1 and R_2 are the charge transfer resistance of the interfaces of the counter electrode/electrolyte and porous electrode/electrolyte, respectively. The finite Warburg impedance related elements, which are associated with diffusion processes, are influenced by the nature of the nanoparticle electrode/electrolyte interface. The symbol, CPE, describes the constant phase element of the capacitance, meaning a non-ideal frequency dependent capacitance due to a non-uniform distribution of current by the material heterogeneity [28]. The elements with subscripts 1 and 2 are related to the capacitance of the interfaces of the electrolyte/Pt-coated counter electrode and photoelectrode/electrolyte, respectively. The CPE was defined by two values, CPE-T and CPE-P.

$$Z = \frac{1}{[T * (j\omega)^P]}$$

T and P were abbreviated as CPE-T and CPE-P, respectively. CPE-P is a constant ranging from $0 \le p \le 1$. A rough or porous surface can cause a double-layer capacitance to appear as a constant phase element with a CPE-P value between 0.9 and 1. The finite Warburg impedance (W_s), which depends on the parameters, W_s–R, W_s–T and W_s–P, accounts for the finite-length Warburg diffusion (Z_{Dif}) in one dimension. In the diffusion interpretation, W_s–$P = l^2/D$, where l is the effective diffusion thickness (approximately 60 μm) and D is the effective diffusion coefficient of the species [29]. Z_{Dif} is defined as follows:

$$Z_{Dif} = \frac{R_{Dif} * \tanh (jT\omega)^P}{(jT\omega)^P}$$

R, T, and P were abbreviated from W_s–R, W_s–T, and W_s–T, respectively. The DSSCs are complex systems that may involve a variety of reactions at several interfaces. The measured EIS spectrum is similar to the previously reported EIS spectrum, which showed three semicircles in the Nyquist plot. Therefore, the spectra shown in Fig. 4 were fitted to the corresponding equivalent circuits by the ZView software.

Table 2 summarizes the quantitatively fitted results using the equivalent circuit. R_s and R_{Dif} describe the electrolyte resistance and diffusion related resistance of the electrolyte. The control sample showed a R_s, R_{Dif}, R_1 and R_2 of 19.2, 66, 14 and 67 Ω, respectively. On the other hand, 10 wt% LS sample shows less resistance for all the elements (R_s = 18.5 Ω of, R_{Dif} = 49.25 Ω, R_1 = 10 Ω of, and R_2 = 55 Ω). The diffusion coefficient (D) of I_3^- ions was calculated using the equation, W_s–$T = l^2/D$. The diffusion coefficients (D) of the control and 10 wt% LS samples were approximately 3.67×10^{-7} and 9.35×10^{-7} cm^2/s, respectively. This means that the permeation of the polymer electrolyte was supported by the widely distributed

Table 2
Parameters determined by fitting the electrochemical impedance spectra under the open-circuit condition (illumination intensity: 100 mW/cm^2)

	R_S (Ω)	R_{Dif} (Ω)	R_1 (Ω)	R_2 (Ω)	CPE1		CPE2		Diffusion coefficient (cm^2/s)	Film thickness (μm)
					T	P	T	P		
Control sample	19.2	66	14	67	0.00182	0.755	0.00334	0.9385	3.69×10^{-7}	4.7
10 wt% LS	18.5	49.3	10	55	0.0011	0.78	0.0021	0.965	9.35×10^{-7}	5.2

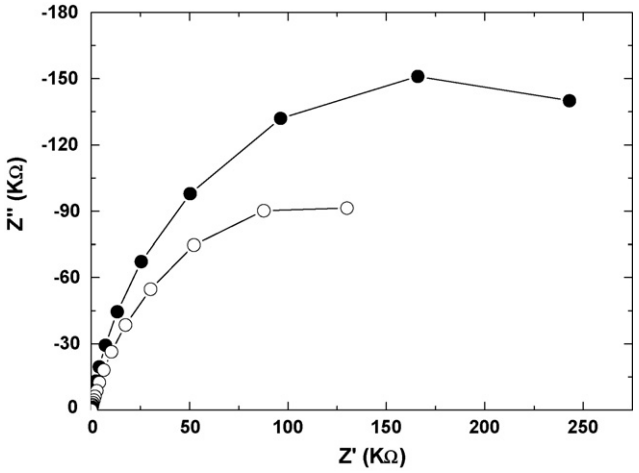

Fig. 5. Impedance spectra measured in the dark at the open-circuit voltage (−0.24 V) shown in the Nyquist diagrams. The control sample and 10 wt% LS sample were described with the filled circle and open circle, respectively.

bulky-pores, which affected the electron transport/transfer phenomenon in the interface region. Moreover, 10 wt% LS sample showed a lower surface area, which influenced the double-layer capacitance. It was assumed that CPE2 is associated with the double-layer capacitance of the TiO_2 film with a CPE-P value ranging from 0.9 to 1. From this, the capacitance of the interface between the nanoporous TiO_2 film and electrolyte could be calculated. Compared with the control sample (182 μF/cm^2), the 10 wt% LS sample shows a lower double-layer capacitance (110 μF/cm^2) due to the incorporation of solid light scattering particles.

Fig. 5 shows the electrochemical impedance spectra measured in the dark state. The control sample showed high impedance over the entire frequency range, while the 10 wt% LS sample showed less resistive properties. The high impedance of both samples was caused by the large resistance of the porous TiO_2 electrode. From an analysis of the impedance spectra, the incorporation of a small amount of large-sized scattering particles in the TiO_2 slurry influences both the diffusion of the viscous polymer electrolyte and the electron transfer of photoinjected electrons in the interconnected TiO_2 network.

An understanding of the electron transport and charge recombination characteristics is needed to investigate the significantly degraded efficiency of the 20 wt% LS sample even though there was an increase in light absorbance. SLIM-PCV under front side illumination was used to measure the electron diffusion coefficients (D) and lifetimes (τ) of many samples.

Fig. 6(a) shows the D values as a function of J_{sc}. Generally, it was expected that higher D values may be produced in the LS inserted TiO_2 films because of the fewer grain boundaries. This should result in a lower resistance to the photoinjected electrons transferring through the nanoporous TiO_2 electrode if the electrons are transported by a hopping mechanism [30]. However, the 10 wt% LS incorporated TiO_2 films showed lower diffusion coefficients, compared with the TiO_2 film without the LS particles.

In particular, the electron transport characteristics of the 20 wt% LS samples were much lower. The addition of materials synthesized in the different circumstances to the nanoporous TiO_2 film resulted in increased resistance due to unfavorable matching at the interface between the nanoparticles [31]. This effect was revealed when the fraction of LS particles in the samples was increased. The trend of electron lifetime as a function of J_{sc} was also similar to that of the D values measured for each sample, as shown in Fig. 6(b). The electron lifetimes were reduced with increasing content of LS particles in the

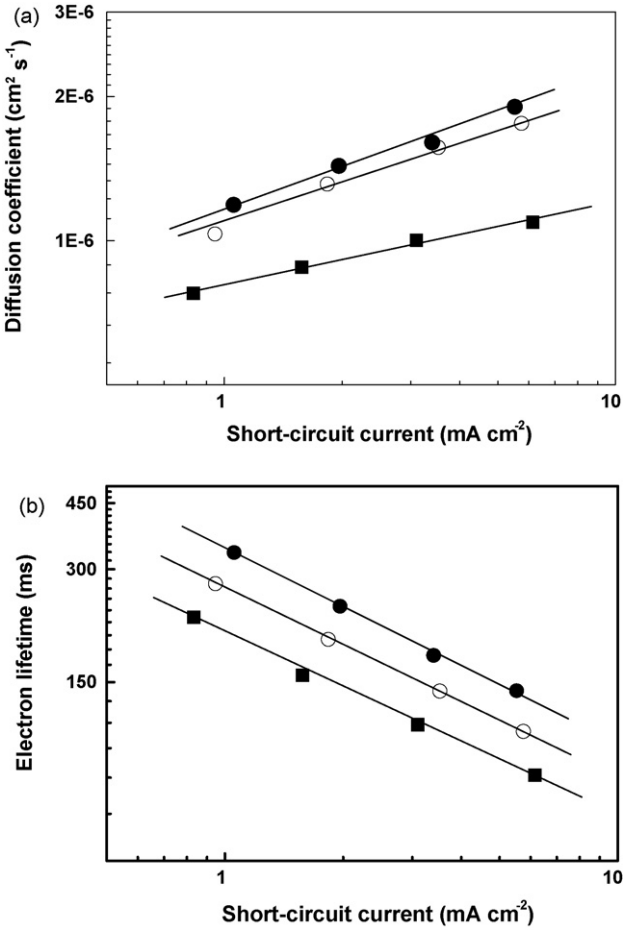

Fig. 6. The values of the electron diffusion coefficients (a) and electron recombination lifetimes (b) as a function of the J_{sc} value controlled by ND filters using a 635 laser beam. The control sample (●) with 5.67 μm, 10 wt% LS sample (○) with 4.7 μm, and 20 wt% LS sample (■) with 6.81 μm are shown.

TiO_2 powder, presumably by the contribution of electrons remaining in the grain boundaries [32]. This shows that there was a minor increase in conversion efficiency in the 10 wt% sample despite the degraded electron transport and charge recombination properties, particularly where there was high light absorbance at the longer wavelengths corresponding to an increase in J_{sc}. In particular, the considerably lower efficiency in the 20 wt% LS samples was associated with inferior electron transport and recombination properties, despite the enormous light absorbance.

In summary, the optimum condition for high conversion efficiency was a TiO_2 film containing 10 wt% light scattering particles. The 10 wt% LS sample had a suitable combination of minor losses in electron transport and charge recombination as well as increased light absorbance, which would lead to higher efficiency.

4. Conclusions

This paper reports the first attempt to fabricate a solid-state DSSC using modified TiO_2 films containing porous inducing materials, *i.e.*, large-sized light scattering particle and polymer beads, which improve the diffusion of a solid-state polymer electrolyte into the nanostructured TiO_2 film and together increase J_{sc} due to a light scattering effect in the longer wavelength range. The maximum absorption wavelength of the dye was shifted toward a longer wavelength as more solid light scattering particles were incorporated while there was no enhancement in the absorbance in the

case of the PB incorporated TiO_2 film. However, the cell efficiency was degraded when the content of incorporated LS was increased because of the decreased surface area, the reduced electron transport and increased charge recombination. Lower efficiency was always observed in the case of the incorporated polymer beads. The optimum amount of LS particles incorporated was approximately 10 wt% by weight, showing the highest performance of 4.75% (0.651 V of V_{oc}, 12.6 mA/cm^2 of J_{sc}, and 0.58% of fill factor). The diffusion properties of the solid polymer electrolyte examined using electrochemical impedance spectroscopy revealed the 10 wt% LS sample to show favorable diffusion of the polymer electrolyte and lower resistance at the interface photoanode/electrolyte. The porous TiO_2 films containing the 10 wt% light scattering particles enabled easy diffusion of the polymer electrolyte. These results suggest that TiO_2 films containing 10 wt% light scattering particles can be applied to solid-state DSSCs.

Acknowledgements

This work was supported in part by KOSEF (Contract No. R01-2004-000-10143-0), and in part by the Research Center for Energy Conversion and Storage (Contract No. R11-2002-102-00000-0).

References

[1] B. O'Regan, M. Grätzel, Nat. (Lond.) 353 (1991) 737–740.
[2] E. Stathatos, P. Lianos, Adv. Mater. 13 (2002) 350–354.
[3] B. Li, L. Wang, B. Kang, P. Wang, Y. Qiu, Sol. Energy Mat. Sol. Cells 90 (2006) 549–573.
[4] A.F. Nogueira, C. Longo, M.-A. De Paoli, Coord. Chem. Rev. 248 (2004) 1455–1468.
[5] P. Wang, S.M. Zakeeruddin, P. Comte, I. Exnar, M. Grätzel, J. Am. Chem. Soc. 125 (2003) 1166–1167.
[6] U. Bach, Y. Tachibana, J.E. Moser, S.A. Haque, J.R. Durrant, M. Grätzel, D.R. Klug, J. Am. Chem. Soc. 121 (1999) 7445–7446.
[7] K.-S. Ahn, Y.-C. Nah, J.-Y. Park, Y.-E. Sung, K.-Y. Cho, S.-S. Shin, J.-K. Park, Appl. Phys. Lett. 82 (2003) 3379–3381.
[8] S.-E. Cheon, J.-H. Cho, K.-S. Ko, C.-W. Kwon, D.-R. Chang, H.-T. Kim, S.-W. Kim, J. Electrochem. Soc. 149 (2002) A1437–A1441.
[9] H. Zhang, S. Kulkarni, S.L. Wunder, J. Electrochem. Soc. 153 (2006) A239–A248.
[10] K.-Y. Cho, J.-Y. Eom, N.-S. Choi, Y.-M. Lee, J.-K. Park, J.-H. Choi, K.-W. Park, Y.-E. Sung, Electrochim. Acta 50 (2004) 583–593.
[11] S.H. Kang, J.-Y. Kim, Y.-E. Sung, J. Photochem. Photobiol. A: Chem. 186 (2007) 234–241.
[12] Y. Tachibana, K. Hara, K. Sayama, Chem. Mater. 14 (2002) 2527–2535.
[13] K. Hara, K. Miyamoto, Y. Abe, M. Yanagida, J. Phys. Chem. B 109 (2005) 23776–23778.
[14] Hyung-Jun Koo, Yong Joo Kim, Yoon Hee Lee, Wan In Lee, Kyungkon Kim, Nam-Gyu Park, Adv. Mater. 20 (2008) 195–199.
[15] Yong Zhao, Jin Zhai, Tianxin Wei, Lei Jiang, Daoben Zhu, J. Mater. Chem. 17 (2007) 5084–5089.
[16] S.H. Kang, J.-Y. Kim, Y.-E. Sung, Electrochim. Acta 52 (2007) 5242–5250.
[17] S. Nishimura, N. Abrams, B.A. Lewis, L.I. Halaoui, A.J. Frank, J. Am. Chem. Soc. 125 (2003) 6306–6310.
[18] H.-D. Koh, J.-S. Lee, Macromol. Rapid Commun. 28 (2007) 315–321.
[19] J.H. Kim, M.-S. Kang, Y.J. Kim, Y.S. Kang, Chem. Commun. (Cambridge) (2004) 1662–1663.
[20] S. Nakade, T. Kanzaki, Y. Wada, S. Yanagida, Langmuir 21 (2005) 10803–10807.
[21] Soon Hyung Kang, Sang-Hyun Choi, Moon-Sung Kang, Jae-Yup Kim, Hyun-Sik Kim, Taeghwan Hyeon, Yung-Eun Sung, Adv. Mater. 20 (2008) 54–58.
[22] S. Hore, R. Kern, Chem. Commun. (Cambridge) (2005) 2011–2012.
[23] A. Usami, Chem. Phys. Lett. 277 (1997) 105–108.
[24] S. Hore, C. Vetter, R. Kern, H. Smit, A. Hinsch, Sol. Energy Mat. Sol. Cells 90 (2006) 1176–1188.
[25] K.D. Benkstein, N. Kopidakis, A.J. Frank, J. Phys. Chem. B 107 (2003) 7759–7767.
[26] T.-S. Kang, K.-H. Chun, J.S. Hong, S.-H. Moon, K.-J. Kim, J. Electrochem. Soc. 147 (2000) 3049–3053.
[27] C. Longo, A.F. Nogueira, M.-A. De Paoli, H. Cachet, J. Phys. Chem. B 106 (2002) 5925–5930.
[28] Q. Wang, J.-E. Moser, M. Grätzel, J. Phys. Chem. B 109 (2005) 14945–14953.
[29] M. Adach, M. Sakamoto, J. Jiu, Y. Ogata, S. Isoda, J. Phys. Chem. B 110 (2006) 13872–13880.
[30] J. Bisquert, J. Phys. Chem. B 108 (2004) 2323–2332.
[31] Z.-S. Wang, H. Kawauchi, T. Kashima, H. Arakawa, Coord. Chem. Rev. 248 (2004) 1381–1389.
[32] M.J. Cass, Alison B. Walker, D. Martinez, L.M. Peter, J. Phys. Chem. B 109 (2005) 5100–5107.